

Simulation of finite element model of surface pit on f304 stainless steel

Surinder Pal

Research Scholer,

Department of Industrial and Production Engineering,

Dr. B R Ambedkar National Institute of Technology Jalandhar, Punjab, India

Email: Surinder92.pal@gmail.com

Abstract

The present study is directed on the FEA simulation of the hemispherical pits of F304 Stainless steel using Abaqus 6.14. The three-dimensional modeling of hemispherical pits was created at different diameters. The applied load was 60%, 75% and 90% of the yield stress of F304 stainless steel. Thus five hemispherical pits were created in the center of the rectangular plate at different depths and diameters. This study exhibited the diameter elongation of pits, von Mises stresses, and Max principal stresses. Furthermore, the reported results herein should be appropriate for the uncertainty of damage and elongations of pits and of degrading the material strength for f304 stainless steel at different applied loads. The sub modeling techniques have been employed to compare the simulated results with analytical results. Consequently, the results of this study suggest the critical regions of maximum stress concentration for various types of pits mainly around the pit surface, including depth and diameters.

Keywords: *F304 Stainless steel, pit, corrosion, Abaqus.*

INTRODUCTION

The primitive application of F304 stainless steel to all sorts of industrial and domestic especially in valves. To evaluate the maximum stress concentration around the hemispherical pits, the current study was performed with the help of Finite element analysis. It consists of several types of hemispherical pits at the center of the rectangular plate at varying applied load. Numerous researchers demonstrated the combined effect of pitting with applied stress to examine the stress concentration factor. It is also known as stress corrosion cracking (SCC). The SCC is a materials degradation mechanism also known to affect the stainless steels and can commence to an unexpected failure of generally ductile metals. The functional and structural integrity of materials utilized in corrosive atmospheres is a critical concern as unpredicted failure could have severe consequences [1]. Corrosion pits are most likely to initiate

the localities of stress corrosion cracking [2]. Once they start, they rise the local stress concentrations in the presence of remote stresses [3].

Additionally, the corrosion pits have mixed types of shapes such as elliptical, circular, shallow and wide, deep and narrow, and vertical or horizontal [4]. These shapes directly influence the stress concentrations, and the outcomes of such stress concentrations can affect the growth of cracks from areas of high-stress concentration initially. The mechanisms of stress corrosion cracking can also result in cracks by when the applied stresses result more notable than the required thresholds for stress corrosion cracking [5]. The presence of chlorides shows the common environmental exposure condition responsible for SCC of stainless steels. Even though no grade of stainless steel is entirely immune to chloride SCC [6]. The stress corrosion cracking induced by the

combined effect of tensile stress and corrosive atmosphere. The influence of SCC on material typically falls between the dry cracking and fatigue threshold of that material. The required tensile stresses may be directly applied to stresses or in the form of residual stresses [7].

The Pitting corrosion is the risk form of localized corrosion, causing the loss of metal. The present analysis is concerned with the investigation of the risk of damage around the pits and elongations of pits diameter by applied pressure. It has been noted that for the assumed ideal elastic-plastic material the shape and volume of the plastic field depend on pit depth and its geometry [8]. Thus, the pits geometry has been developed with the help of Abaqus. The pits shaped were hemispherical which incorporate the depth and diameter.

Furthermore, when the chloride ions surpass a critical concentration, the passive film could be cracked to create pitting corrosion [9]. Recent results show that the nucleation of the corrosion pit arises from a microscopically violent event, detected as a sharp small current transient which initiates metastable pit growth [10]. Corrosion of stainless steels, including the austenitic Fe-Cr-Ni alloys, is related with MnS inclusions that bring local sites for corrosion pits. The considerable research effort has been concentrated on the role of MnS in corrosion of cast and wrought stainless steel to date, containing microanalysis of MnS and the nearby

microchemistry [11]. The pitting corrosion with the additional localized attack, rising, particularly in depth. The Corrosion characterization has been limited to corrosion rate valuations derived from either weight loss or electrochemical procedures, which has turned into routine repetition in quantifying aqueous Corrosion rates [12].

Moreover, pitting corrosion is the principal cause of steel failure in corrosive atmospheres. Pitting typically appears in a minor area of the metal surface and initiates stress corrosion cracking [13,14]. Turnbull et al. studied finite element analysis to determine the stress, and strain distribution related to a corrosion pit in a cylindrical steel sample stressed in tension. This view presents the Simulation of a rising pit in a static stress field specified corresponding plastic strain rates that were proportionate with values linked to stress corrosion cracking [15]. The finite element analysis is a handy tool to determine stresses induced in various materials [16]. Pidaparti et al. specified that the stresses increase by 80% within the first 30 min corrosion and then increased by about 6% from 30 min to 60 min and reach a plateau. From certain stresses, it is possible to evaluate the initiation of cracks, from which life can be estimated for failure in the material [17]. The prime focus of this study to understand the behavior of pits using FEA, and described the von Mis es stress, Max Principle stress, the elongation of diameter in the pit center and throughout the plate respectively.

Mechanical properties and chemical compositions of F304 stainless steel Material Properties.

Table 1: Chemical composition

Carbon	Silicon	Manganese	Phosphorous	Sulphur	Chromium	Nickel	Nitrogen
0.08% Max.	0.75% Max.	2.00% Max.	0.045% Max.	0.03% Max.	18-20% Max.	8-12% Max.	0.10% Max.

Table 2: Mechanical properties solution annealed condition

Yield	Tensile Strength	Elongation	Hardness
205 MPa Min	515 MPa Min	30% Min	215 HB Max

3D Geometry

The dimensions of the specimen were classified as per the standard of ASTM G48 method. Fig 1 displays the geometry of a rectangular part with the central pit and the dimensions of the rectangular plate were 50.49mm × 25.73mm × 3.09mm. The Tet mesh has been applied to mesh the rectangular plate. The complete 47981 number of

elements have been formed during meshing. The C3D10 Element Type was applied for analysis. This element is recommended explicitly for fully automatic tetrahedral meshes. To make the mesh denser, seeding method has been implemented around the pits. Fig 5 (i) shows the seeding around the pits in which a 50 to 60 number of the element placed nearby the pit surface.

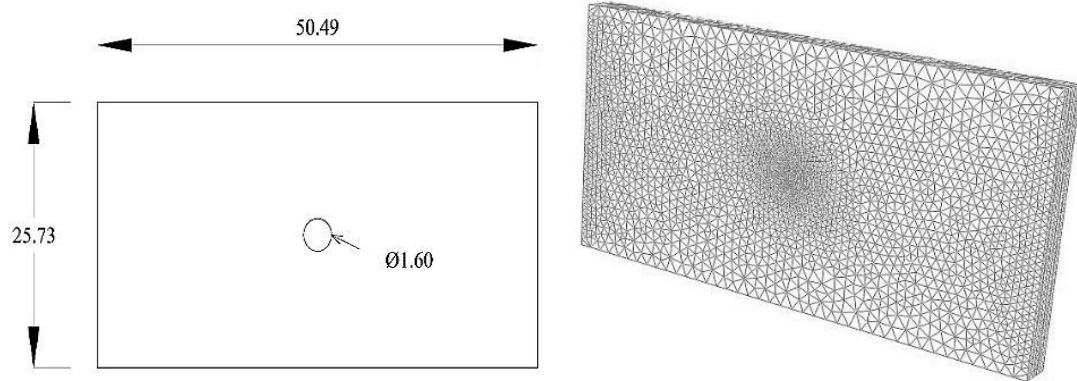


Figure 1: 3d geometry of Rectangular plate with the central pit.

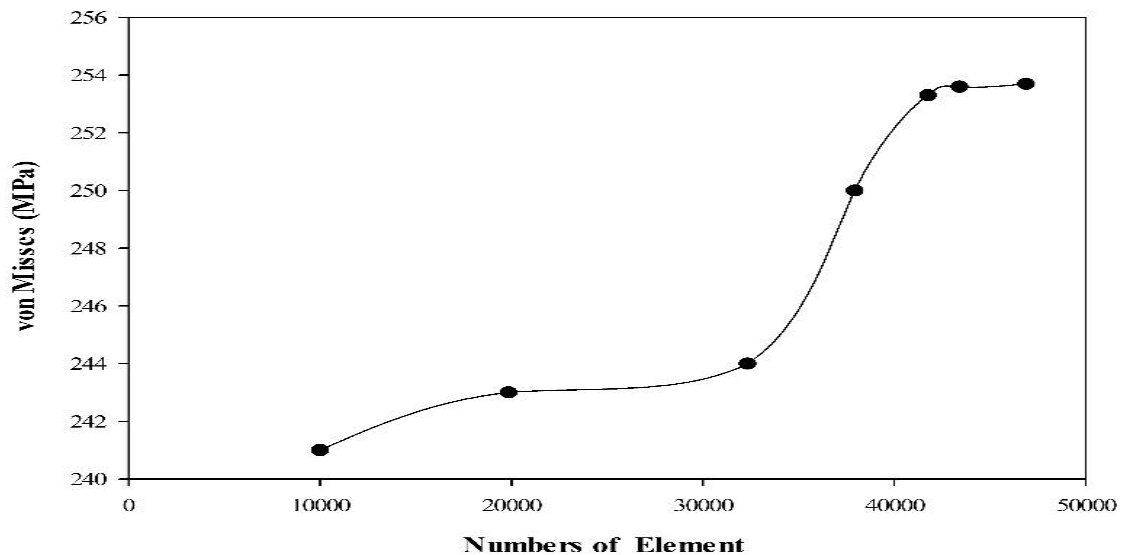


Figure 2: Mesh Convergence.

Simulation Methodology

The simulation methodology introduces the 3D geometry and set of parameters such as load, material properties, and boundary condition. Fig 3. shows the

Flowchart of FEA Process. At the outcome of the simulation, the von-Misses and Max principal stresses around the pits have been determined.

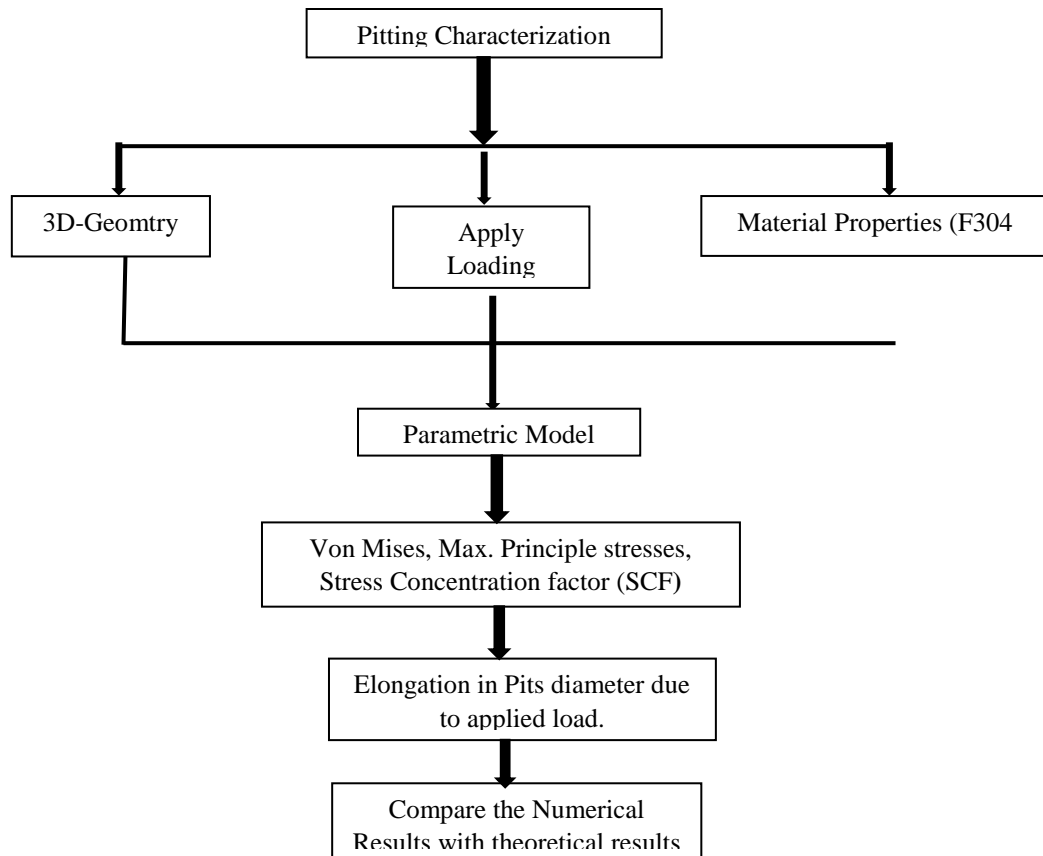


Figure 3: Simulation Methodology flow chart

Finite Element Analysis and Discussion

The simulation results were carried out at several pit sizes. The first simulation was run using a rectangular plate with a pit size of 1.60 mm. The simulation

outcomes confirm the von-Mises stresses at an applied load of 123MPa, 153MPa, and 184MPa respectively..Thus, the other pits also have been examined.

Table 3: FEA Simulation results for different size of pits.

S.No	Pit Size (mm)	Applied Load (MPa)	Von-Mises (Through out the plate) (MPa)	Von-Mises (at pit center) (MPa)	Principal Stress (Through out the plate) (MPa)	Principal Stress (at pit center) (MPa)	Pit Elongation. (mm)
1	1.60	123	254	188	285	240	1.614
2	1.60	153	317	264	375	319	1.615
3	1.60	184	381	350	428	380	1.617
4	0.72	123	248	193	286	220	0.722
5	0.72	153	311	242	358	313	0.723
6	0.72	184	373	358	429	366	0.732
7	0.48	123	249	193	309	207	0.482
8	0.48	153	312	256	387	310	0.483
9	0.48	184	374	272	464	312	0.491
10	1.88	123	257	247	315	250	1.894
11	1.88	153	322	313	394	315	1.933
12	1.88	184	387	370	473	385	1.939
13	2.60	123	263	252	275	266	2.603
14	2.60	153	333	320	343	329	2.721
15	2.60	184	400	390	417	382	2.794
16	0.40	123	248	243	308	188	0.405
17	0.40	153	310	297	385	270	0.491
18	0.40	184	372	357	462	366	0.511

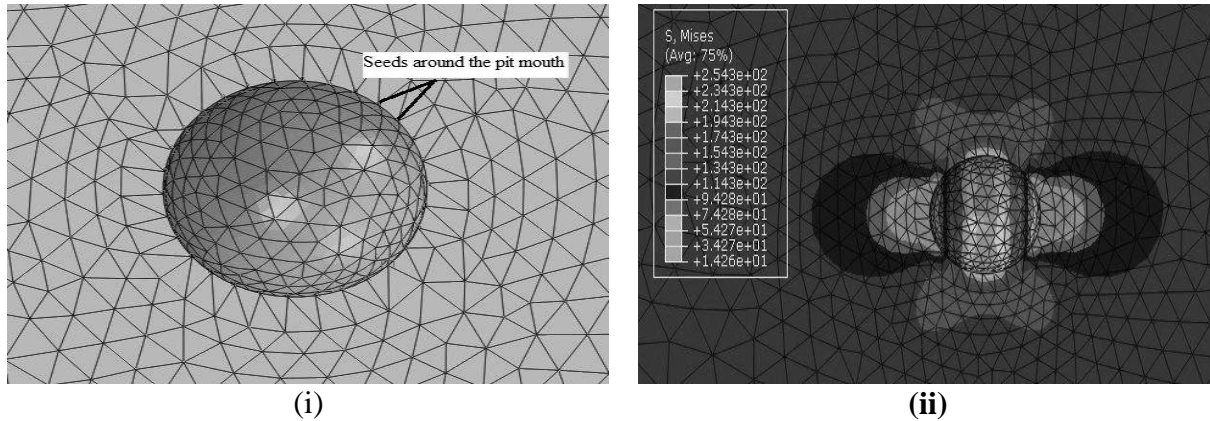


Figure 4: (i) Mesh density around a pit (ii) Pit size 1.6mm and applied load at 123

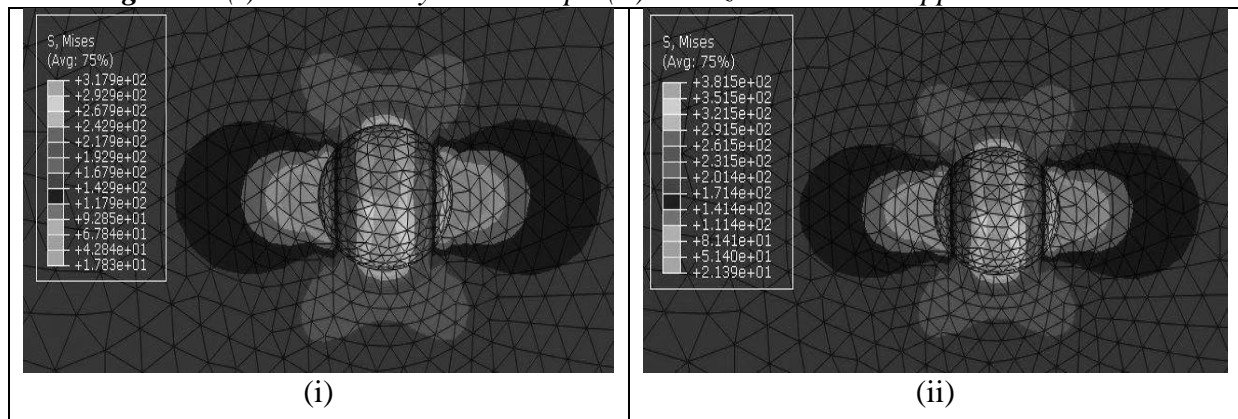


Figure 5: Pit size 1.6mm and applied load at 153 MPa **Figure 6:** Pit size 1.6mm and applied load at 184.5 MPa.

The results of stress distribution were non-uniform. It has been identified with the help of pit shape and geometry. Fig. 4 (i) shows the reliable number of seeds on the edge of pit mouth, which was determined to be 30 by element size. Results intimate the pit growth is directly proportional to tensile loading. Moreover, the induced stress on the

model is higher than the applied stress. Fig 4 (ii), 5 and 6 show the Von-misses at 123 MPa, 153 MPa, and 184.5 MPa respectively. The pits which are having small diameter record higher Von-misses stresses. Moreover, the pit location and depth are the critical factors to expecting the appearance of the maximum stress on the surface.

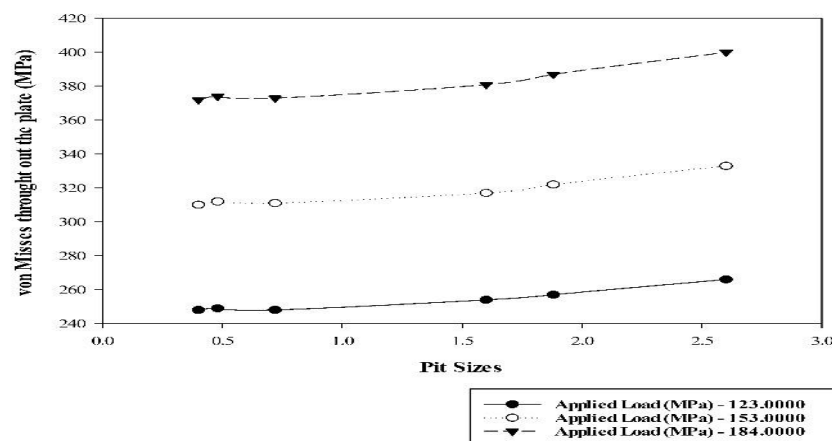


Figure 7: Pit size vs. von Mises throughout the plate.

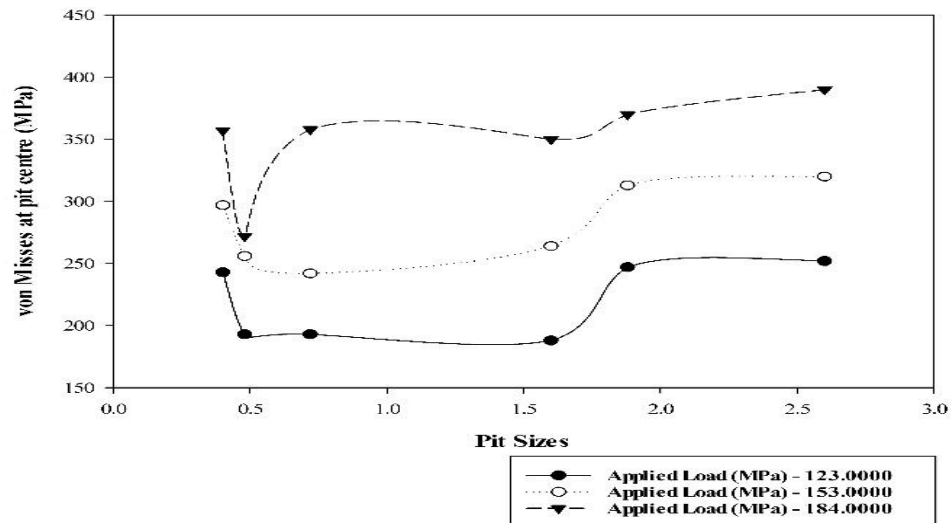


Figure 8: Pit size vs. von Mises at the pit center.

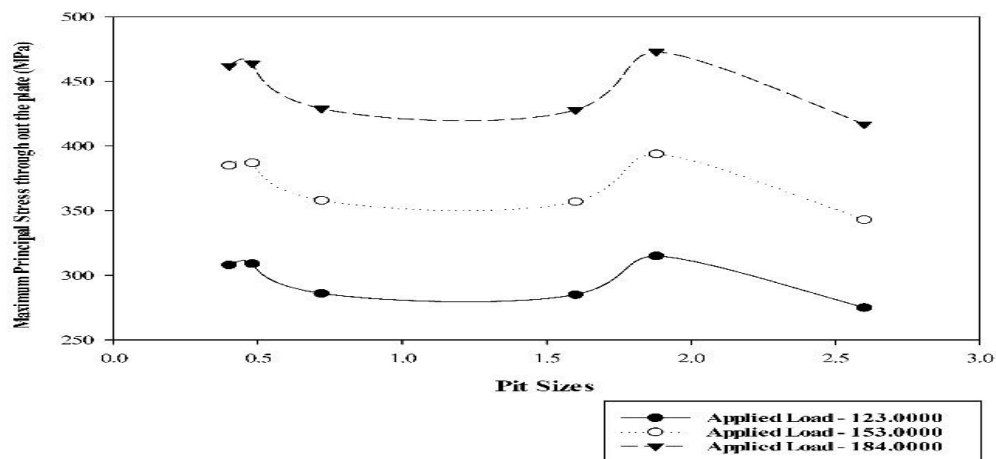


Figure 9: Pit size vs. Max. Principal Stress throughout the plate.

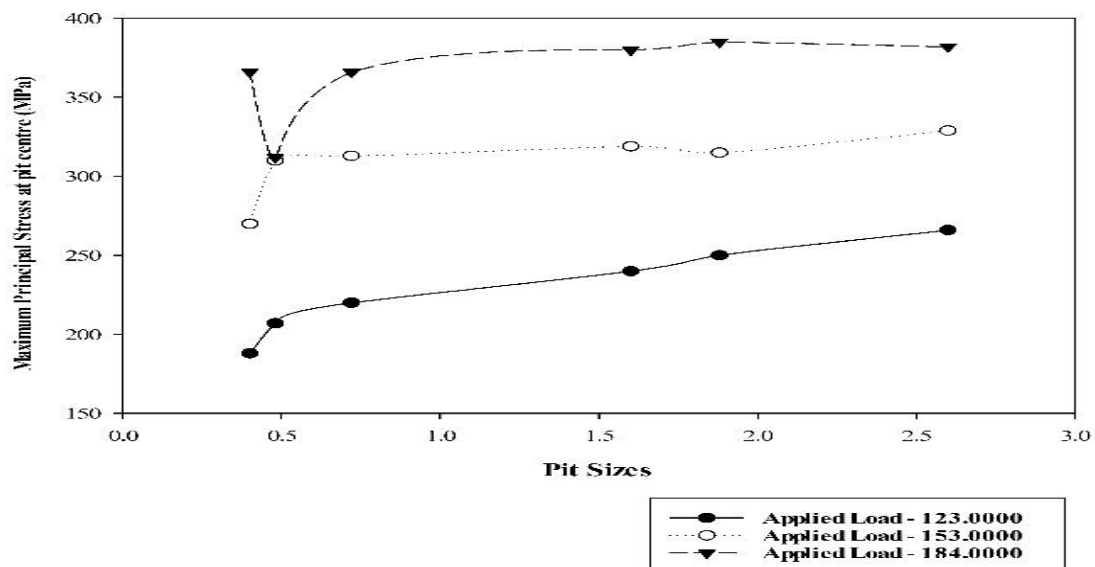


Figure 10: Pit size vs. Max. Principal Stress at pit center.

The figs 7,8, 9 10 shows, the distribution of the stress of pit valleys. The Maximum stress sites of samples vary by changing the pit profile and size. Moreover, the effect of the Maximum principal stress seen in Fig 10 to replicate that the pit size critically affects the distribution of stress around the pit surface.

Overall, the pit to crack transitions depends on the direction of applied loading as well as on pit morphology. Cerit M. studied that any premature pit

formation can cause crack initiation under mechanical loading [18]. Furthermore, it was evident in fig 11 that the elongation of pits diameter raised along with von Mises stresses. However, a very low variation has been noted in von Mises from the pit size of 0.2 mm to 1 mm. It was also observed that the von Mises stresses high in a small pit diameter. Additionally, the Max principal stresses raised with an increase in the elongation of pits diameters shown in fig 14.

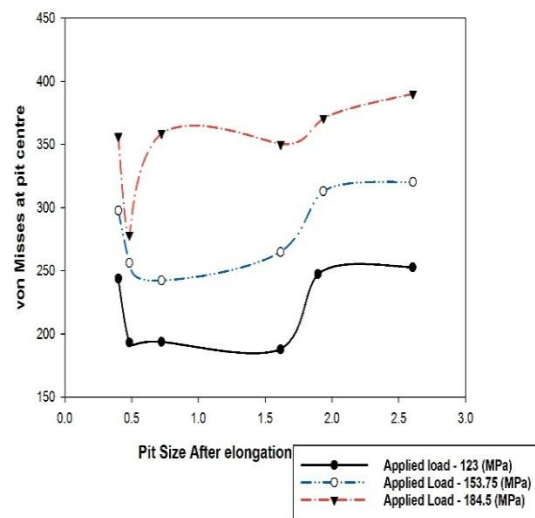
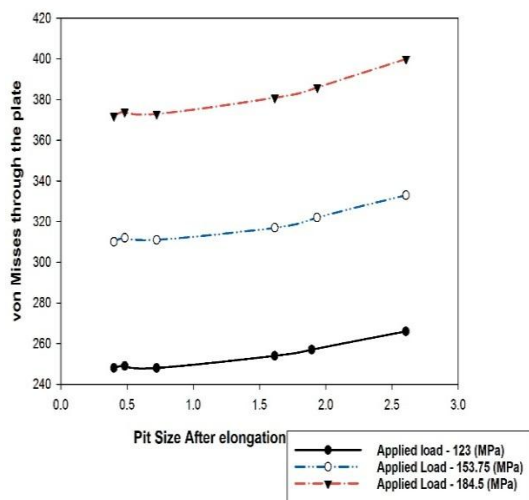


Figure 11: Pit size elongation vs. von Mises Stress. **Figure 12:** Pit size elongation vs. von Mises at pit center.

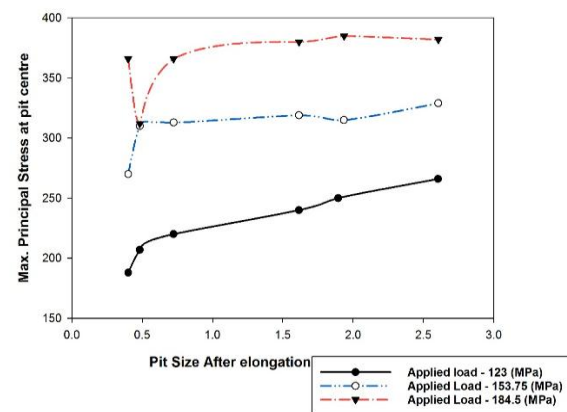
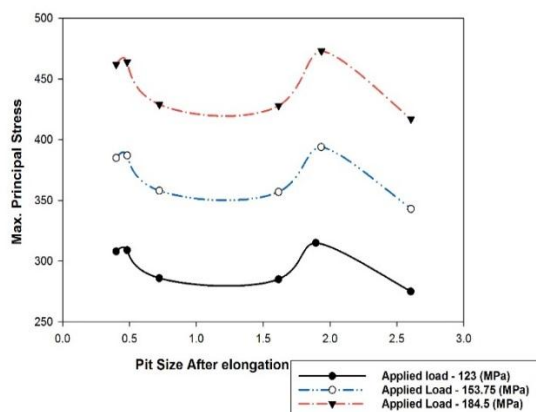


Figure 13: Pit size elongation vs Max. Principal Stress. **Figure 14:** Pit size elongation vs Max. Principal stress at pit center

FEA Model of a circular pit with crack or without crack

To find the stress concentration at the crack

tip a single pit of 1.6mm size has been analyzed for further investigation. Section (a) shows the pits pit without any crack and (b)

shows the same pit in which a small crack has been developed at the bottom as shown in

Fig.15.

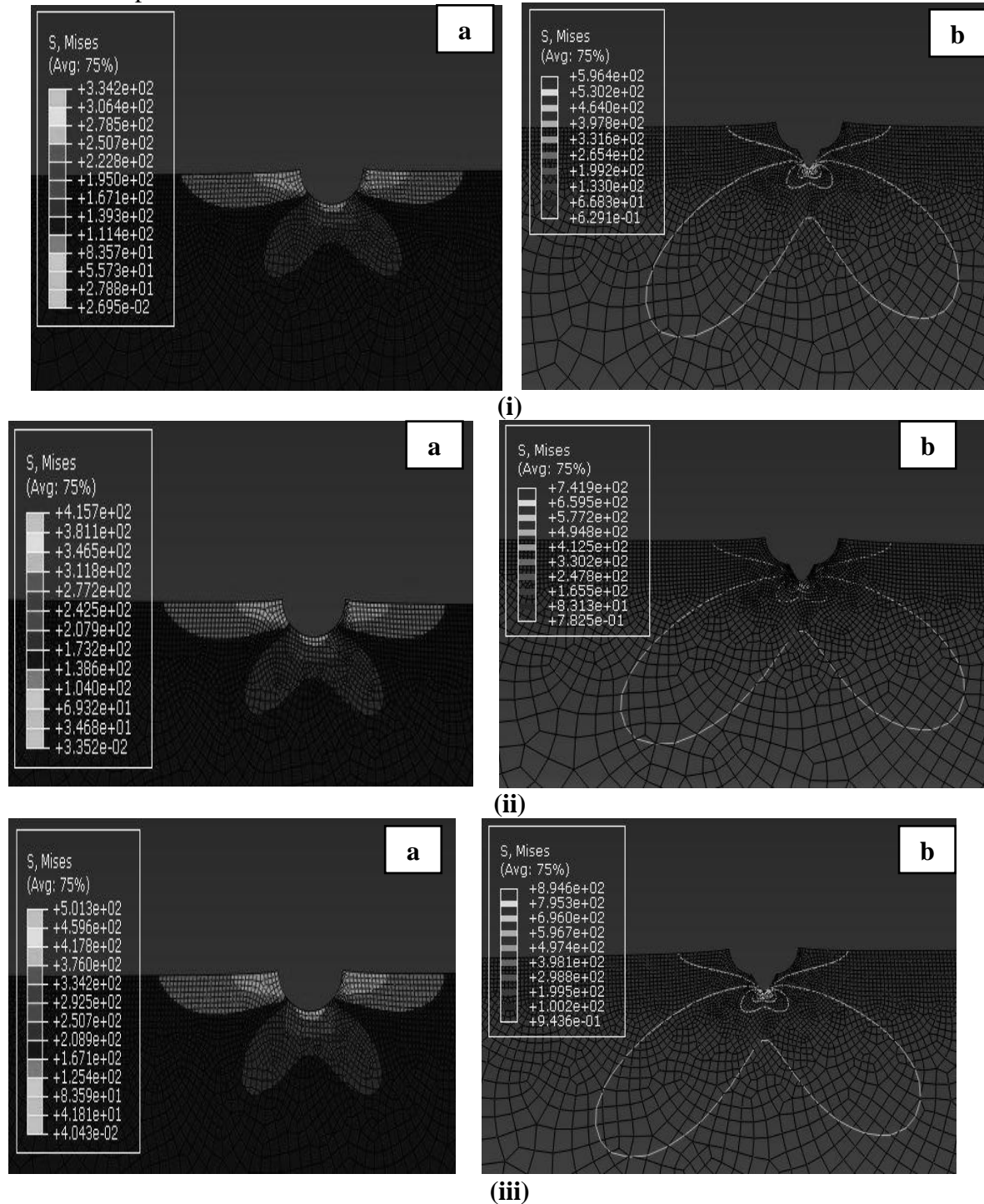


Figure 15: Finite element model of the circular pit (a) without a crack and (b) with a crack at and (i) with a stress of 123 MPa, (ii) with a stress of 153 MPa, and (iii) with a stress of 184.5MPa respectively.

The resultant of Finite element models gives the maximum stress concentration at the bottom of the pit. Fig. 15 depicts the

simulation results for the hemispherical pits for (a) without crack and (b) with a crack. As the Stress Concentration Factor increased, the

individual pits compound to form a bigger pit. The critical stress condition of pits also reached which were responsible for the transition of the pit to a crack.

Pit Driving Forces

The stresses at the tip of the pits were determined to investigate whether the pits can propagate or not. The stress intensity factor (K) is given by [19]:

$$K = y\sigma\sqrt{\pi a}$$

Where K is the stress intensity factor, σ is applied stress, a is the pit size, and Y is a dimensionless parameter. Hence, subcritical crack growth will occur when $K \geq K_{th}$. The following table show the stress intensity factor for the different size of pits along with an applied loads.

Table 4: Stress Intensity factor for the different size of pits diameters.

SNo.	Applied Load (MPa)	Pit diameter = a (mm)	y	Stress Intensity Factor (MPa)
1	123	0.4	1.12	154
2	153	0.4	1.12	192
3	184.5	0.4	1.12	231
4	123	2.6	1.12	393
5	153	2.6	1.12	488
6	184.5	2.6	1.12	588
7	123	0.48	1.12	169
8	153	0.48	1.12	209
9	184.5	0.48	1.12	252
10	123	0.72	1.12	207
11	153	0.72	1.12	257
12	184.5	0.72	1.12	309
13	123	1.6	1.12	308
14	153	1.6	1.12	383
15	184.5	1.6	1.12	462
16	123	1.8	1.12	327
17	153	1.8	1.12	406
18	184.5	1.8	1.12	489

Theoretical calculation of Max. stress of pit placed in the rectangular plate.

The sub modeling method has been applied to analyzing the simulation results with theoretical results. On behalf of the case of a central pit in a rectangular plate, the stress concentration Factor was computed using $(d/D) = (1.61\text{mm}/25.73\text{mm})$. Mainly, the material is stronger when it is entirely free from holes and cracks. Such a perfect material will have a similar strength as theoretically determined. However, holes and sharp corners show the stress concentration factor which presenting the information regarding the extreme magnitude of stress and a sudden turning and the accumulation of more quantum of stress line, especially in the pit region. Mainly, it is a function of the geometry of the component. For the

present study, the thickness of the plate was considered as zero because the maximum stress concentration (SC) was found at the surface of the plate. Therefore, only the surface stress has been investigated for comparing the FEA and theoretical solution. Following equation has been used to find out the stress concentration factor. [20]

$$K_t = 3.0 - 3.140 \left(\frac{d}{D}\right) + 3.667 \left(\frac{d}{D}\right)^2 - 1.527 \left(\frac{d}{D}\right)^3 \quad (1)$$

After calculating Stress Concentration factor (K_t), the Normal stress needs to calculate as follows:

$$\sigma_{nom} = \frac{P}{(D-d)t}$$

P = Load, D = width of the plate, d = pit diameter, t = thickness of the plate.

$$\sigma_{nom} = F \left(\frac{W}{W-d} \right)$$

In this case the W = 25.73mm, F = 123N, 153.75 N and 180.5 N. The Table 5 shown the nominal stress, stress concentration, and max stresses.

Table 5: Comparing the values of maximum stresses of Theoretical results with Abaqus solutions.

S.no	K _t	(d) Pit size mm	Applied Load (MPa)	σ_{nom} (MPa)	K _t (Max = 3)	$\sigma_{max} = k\sigma_{nom}$	Max. Stress (Abaqus)	Error %
1	2.57	1.61	123	130	2.57	334	332	0.005%
2	2.57	1.61	153	162	2.57	416	416	0%
3	2.57	1.61	184	195	2.57	501	501	0%
4	2.90	0.72	123	126	2.90	365	333	8%
5	2.90	0.72	153	158	2.90	458	417	8%
6	2.90	0.72	184	187	2.90	542	498	8%
7	2.94	0.48	123	125	2.94	367	334	8%
8	2.94	0.48	153	154	2.94	452	413	8%
9	2.94	0.48	184	185	2.94	543	509	6%
10	2.74	1.89	123	132	2.74	361	348	3%
11	2.74	1.89	153	163	2.74	446	416	6%
12	2.74	1.89	184	196	2.74	537	504	6%
13	2.95	0.4	123	125	2.95	368	339	7%
14	2.95	0.4	153	154	2.95	454	416	8%
15	2.95	0.4	184	186	2.95	548	510	6%
16	2.64	2.6	123	136	2.64	359	327	8%
17	2.64	2.6	153	169	2.64	446	435	2%
18	2.64	2.6	184	204	2.64	538	517	3%

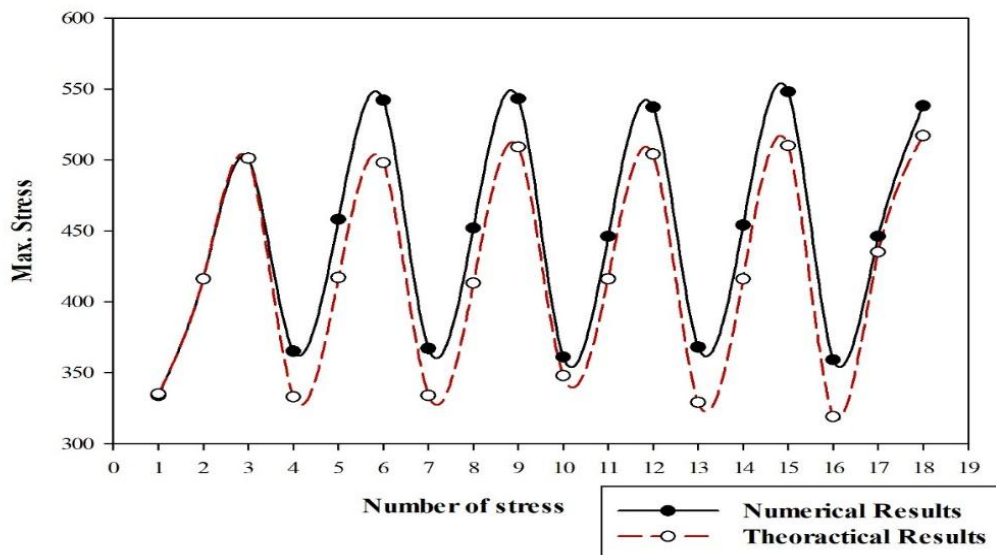


Figure 16: The comparison results of Max. Stress at Theoretical and Numerical Expression.

CONCLUSION

The Numerical Modelling has been used to study the stress distribution around the center pit of the rectangular plate. Besides, the elongation of diameters also studied

along the applied load of 123 MPa, 153 MPa, and 184.5 MPa. The following are the outcomes of the present study:

1. The six cases were studied at varying pit sizes. It was determined that the

maximum stress distribution started around the central pit. The safe stress distribution was observed nearby the pits at 123 MPa. However, at the applied load of 153 MPa and 184.5 MPa, the pit size becomes unstable and may start propagation to crack due to high-stress distribution.

2. The elongation of pit diameter also examined which exhibits directly change in the elongation of pit diameter concerning applied load.
3. The analytical effects have been compared with FEA, and it was determined that the Abaqus shows the accurate results with the maximum error of 8% only (Shown in Table 6).
4. It was found that the stress distribution becomes unpredictable and more intensive around the pit.
5. It has also been noted that the large size of the pit profile, reductions the stress by 66% to 70%.

REFERENCES

1. Cunningham, A., Bottleberghe, J., & Greene, D. (2017). A Method for Detecting Stress Corrosion Cracking and the Influence Environmental Factors.
2. Budinski, K. G. and Budinski, M. K., Engineering Materials, Properties and Selection, 9th ed., Pearson Prentice Hall, Upper Saddle River, NJ, 1986, pp. 133–166.
3. Chen, G. S., Wan, K. C., Gao, M., Wei, R. P., and Flournoy, T. H., "Transition from Pitting to Fatigue Crack Growth-Modeling of Corrosion Fatigue Crack Nucleation in a 2024-T3 Aluminum Alloy," Mater. Sci. Eng., A, Vol. 219, Nos. 1–2, 1996, pp. 126–132, [https://doi.org/10.1016/S0921-5093\(96\)10414-7](https://doi.org/10.1016/S0921-5093(96)10414-7)
4. Pidaparti, R. M., & Patel, R. R. (2008). Correlation between corrosion pits and stresses in Al alloys. *Materials Letters*, 62(30), 4497-4499.
5. Cerit, M., Genel, K., & Eksi, S. (2009). Numerical investigation on stress concentration of corrosion pit. *Engineering Failure Analysis*, 16(7), 2467-2472.
6. <http://www.ssina.com/corrosion/stress-corrosion-cracking.html>
7. [https://www.nace.org/Corrosion-Central/Corrosion-101/Stress-Corrosion-Cracking-\(SCC\)/](https://www.nace.org/Corrosion-Central/Corrosion-101/Stress-Corrosion-Cracking-(SCC)/)
8. Rajabipour, A., & Melchers, R. E. (2013). A numerical study of damage caused by combined pitting corrosion and axial stress in steel pipes. *Corrosion Science*, 76, 292-301.
9. Cheng, C. Q., Klinkenberg, L. I., Ise, Y., Zhao, J., Tada, E., & Nishikata, A. (2017). Pitting corrosion of sensitised type 304 stainless steel under wet–dry cycling condition. *Corrosion Science*, 118, 217-226.
10. Burstein, G. T., Pistorius, P. C., & Mattin, S. P. (1993). The nucleation and growth of corrosion pits on stainless steel. *Corrosion Science*, 35(1-4), 57-62.
11. Chao, Q., Cruz, V., Thomas, S., Birbilis, N., Collins, P., Taylor, A., ... & Fabijanic, D. (2017). On the enhanced corrosion resistance of a selective laser melted austenitic stainless steel. *Scripta Materialia*, 141, 94-98.
12. Örneke, C., Léonard, F., McDonald, S. A., Prajapati, A., Withers, P. J., & Engelberg, D. L. (2018). Time-dependent in situ measurement of atmospheric corrosion rates of duplex stainless steel wires. *npj Materials Degradation*, 2(1), 10.
13. Frankel, G.S. Pitting corrosion of metals-a review of the critical factors. *J. Electrochem. Soc.* 1998, 145, 2186–2198.
14. Newman, R.C. 2001 W.R. Whitney award lecture: Understanding the corrosion stainless steel. *Corrosion* 2001, 57, 1030–1041.

15. Turnbull, A., Wright, L., & Crocker, L. (2010). New insight into the pit-to-crack transition from finite element analysis of the stress and strain distribution around a corrosion pit. *Corrosion Science*, 52(4), 1492-1498.
16. Pawar Pravin (2016). Finite Element Method Analysis of Rectangular Plate with Circular Hole Using Ansys. *Int. J. Chem. Sci.*: 14(4), 2016, 2787-2798.
17. Pidaparti, R. M., & Patel, R. R. (2008). Correlation between corrosion pits and stresses in Al alloys. *Materials Letters*, 62(30), 4497-4499.
18. Cerit, M., Genel, K., & Eksi, S. (2009). Numerical investigation on stress concentration of corrosion pit. *Engineering Failure Analysis*, 16(7), 2467-2472.
19. Hoepfner, D. W., "Model for Prediction of Fatigue Lives Based Upon a Pitting Corrosion Fatigue Process," *Fatigue Mechanisms*, ASTM STP675, J. T. Fong, Ed., ASTM International, West Conshohocken, PA, 1979, pp. 841–870, <https://doi.org/10.1520/STP35917S>.
20. Pilkey, W. D..(2005). *Formulas for Stress, Strain, and Structural Matrices* Formulas for Stress, Strain, and Structural Matrices .2nd Edition John Wiley & Sons